Title

Mutant huntingtin protein induces MLH1 degradation, DNA hyperexcision, and cGAS-STING-dependent apoptosis.

Journal

Proceedings of the National Academy of Sciences, 121(13)

Authors

Sun, Xiao
Liu, Lu
Wu, Chao
et al.

Publication Date

2024-03-26

DOI

10.1073/pnas.2313652121

Peer reviewed

PNAS RESEARCH ARTICLE | CELL BIOLOGY

Mutant huntingtin protein induces MLH1 degradation, DNA hyperexcision, and cGAS–STING-dependent apoptosis

Xiao Sun[a,b,1], Lu Liu[a,1], Chao Wu[a,1], Xueying Li[a], Jinzhen Guo[a], Junqiu Zhang[a], Junhong Guan[c], Nan Wang[d,e], Liya Gu[a], X. Willian Yang[d,e], and Guo-Min Li[a,f,g,2]

Edited by Wei Yang, NIH, Bethesda, MD; received August 18, 2023; accepted January 27, 2024

Huntington's disease (HD) is an inherited neurodegenerative disorder caused by an expanded CAG repeat in the huntingtin (*HTT*) gene. The repeat-expanded *HTT* encodes a mutated HTT (mHTT), which is known to induce DNA double-strand breaks (DSBs), activation of the cGAS–STING pathway, and apoptosis in HD. However, the mechanism by which mHTT triggers these events is unknown. Here, we show that HTT interacts with both exonuclease 1 (Exo1) and MutLα (MLH1–PMS2), a negative regulator of Exo1. While the HTT–Exo1 interaction suppresses the Exo1-catalyzed DNA end resection during DSB repair, the HTT–MutLα interaction functions to stabilize MLH1. However, mHTT displays a significantly reduced interaction with Exo1 or MutLα, thereby losing the ability to regulate Exo1. Thus, cells expressing mHTT exhibit rapid MLH1 degradation and hyperactive DNA excision, which causes severe DNA damage and cytosolic DNA accumulation. This activates the cGAS–STING pathway to mediate apoptosis. Therefore, we have identified unique functions for both HTT and mHTT in modulating DNA repair and the cGAS–STING pathway-mediated apoptosis by interacting with MLH1. Our work elucidates the mechanism by which mHTT causes HD.

Huntington's disease | cGAS-STING | MutLα | Exo1 | mHTT

Huntington's disease (HD) is a progressive neurodegenerative disorder caused by CAG trinucleotide repeat expansions in exon 1 of the huntingtin (*HTT*) gene, which codes the HTT protein (1–3). HD symptoms primarily consist of neuronal death and abnormalities in peripheral tissues. The CAG repeat-expanded *HTT* produces a mutated HTT (mHTT), which displays both loss and toxic gain of functions in comparison with HTT (4–6), including inducing apoptosis in neuronal and peripheral blood cells (7–9). However, the underlying mechanism is unclear.

HD is associated with increased inflammatory mediators in both the central nervous and periphery systems (10–12). Recent studies have implicated the cytosolic DNA sensor cGAS (cyclic GMP-AMP synthase)-triggered innate immune signaling in HD (13, 14). Upon binding to cytosolic DNA, cGAS synthesizes 2′3′-cyclic GMP-AMP (cGAMP), which interacts with and activates the stimulator of interferon genes (STING) to induce type I interferons (IFNs) and cytokines through IRF3/7 and NF-κB, triggering the downstream innate immune response (15–19). The cGAS pathway has been shown to promote an inflammatory response in HD (13), however, the mechanism by which mHTT activates the cGAS–STING pathway is unknown.

The cGAS activation relies on the accumulation of cytosolic DNA triggered by severe chromosome damage (17). HTT participates in ATM-mediated DNA damage response and repair (20, 21), but mHTT impairs such activities, resulting in excessive DNA damage, including double-strand DNA breaks (DSBs) (22–25). DSBs can be repaired by the error-free homologous recombination (HR) pathway, which involves DNA end resection by the 5′ to 3′ exonuclease 1 (Exo1), strand invasion, formation of the Holliday junction, and junction resolution (26–28). DNA end resection by Exo1 is tightly regulated by MutLα, an MLH1–PMS2 heterodimer involved in DNA mismatch repair (MMR) (29). Cells defective in *MLH1* show uncontrolled Exo1-catalyzed end resection, resulting in a large quantity of ssDNAs, accumulation of cytosolic DNA, and activation of the cGAS–STING immune signaling pathway (30). Interestingly, MMR genes, particularly *MSH3* and *MLH1*, have been identified as important genetic modifiers of HD (31–33). The *MSH3* gene product, a subunit of the mismatch recognition protein MutSβ (MSH2-MSH3), acts to promote CAG repeat expansions during DNA replication and repair (34–40). The *MLH1* gene product is also a key driver of the somatic expansion (33), but whether or not MLH1 modulates HD progression through other unknown mechanisms is unknown. Given MutLα's roles in regulating the Exo1-catalyzed end resection and activation of the cGAS–STING pathway in cells expressing mHTT, we hypothesize that MLH1 may play a critical role in mediating HD progression by differentially interacting with HTT and

Significance

Huntington's disease (HD) is caused by CAG repeat-expanded huntingtin (*HTT*), which encodes a mutated HTT (mHTT). The CAG expansion is mediated by the DNA mismatch repair pathway (MMR). However, how mHTT and MMR factors regulate HD onset is unclear. Here, we show that HTT, but not mHTT, interacts with MMR factors MLH1 and exonuclease 1 (Exo1). While the HTT–Exo1 interaction negatively regulates the Exo1-catalyzed DNA excision during DNA repair, the HTT–MLH1 interaction stabilizes MLH1. Thus, mHTT cells exhibit rapid MLH1 degradation and hyperactive DNA excision by Exo1, leading to severe DNA damage and cytosolic DNA accumulation. This activates the cGAS–STING pathway to trigger apoptosis in HD. Therefore, we have identified unique interplays between MMR proteins and HTT/mHTT and the mechanism by which mHTT causes HD.

Author contributions: X.S., L.L., L.G., and G.-M.L. designed research; X.S., L.L., C.W., X.L., and J.Z. performed research; J. Guo and J. Guan generated Mlh1 and Exo1 knockout lines; X.S., L.L., C.W., L.G., and G.-M.L. analyzed data; N.W. and X.W.Y. generated animal models and provided the animal tissues; and X.S., L.L., L.G., and G.-M.L. wrote the paper.

The authors declare no competing interest.

This article is a PNAS Direct Submission.

[1]X.S., L.L., and C.W. contributed equally to this work.

[2]To whom correspondence may be addressed. Email: gmli@cimrbj.ac.cn.

This article contains supporting information online at https://www.pnas.org/lookup/suppl/doi:10.1073/pnas.2313652121/-/DCSupplemental.

Published March 18, 2024.

mHTT, which in turn differentially regulates the Exo1-catalyzed end resection, leading to altered regulation of the cytosolic DNA production and cGAS–STING activation.

We demonstrate here that HTT interacts with both Exo1 and MLH1, with the HTT–Exo1 interaction negatively regulating the Exo1-catalyzed DNA end resection during DSB repair by HR and the HTT–MutLα interaction functioning to stabilize MLH1. In contrast, mHTT shows a much weak interaction with Exo1 and MLH1. Thus, cells expressing mHTT exhibit rapid MLH1 degradation and uncontrolled DNA end resection, which induces severe DNA damage and the accumulation of cytosolic DNA. This activates the cGAS–STING pathway to mediate apoptosis. Therefore, we have identified hitherto unknown functions of both HTT and mHTT in modulating DNA repair and the cGAS–STING pathway-mediated apoptosis by differentially interacting with MLH1.

Results

mHTT-induced Apoptosis Depends on the cGAS–STING Pathway. To determine whether or not mHTT-induced apoptosis in HD is mediated through the cGAS–STING pathway, we knocked out *Sting* or *Cgas* in the mouse striatal-derived cell lines STHdh$^{Q7/Q7}$ and STHdh$^{Q111/Q111}$ (Fig. 1*A*), which contain homozygous *HTT* loci with a humanized exon 1 containing 7 and 111 CAG repeats, respectively (13, 41, 42). The resulting cell lines showed reduced levels of phosphorylated STAT1 (pSTAT1), phosphorylated TBK1 (pTBK1), and phosphorylated STING (pSTING) (Fig. 1*A*). Cell viability analysis using the MTS assay (43) revealed that STHdh$^{Q111/Q111}$ cells displayed a survival rate that is significantly lower than that of STHdh$^{Q7/Q7}$ cells (Fig. 1*B*), suggesting that cells expressing mHTT undergo apoptosis. This was confirmed by the Annexin V Apoptosis Assay performed with cells treated for 12 h of serum deprivation (44–46), as the percentage of apoptotic cells in STHdh$^{Q111/Q111}$ cells was significantly higher than that in STHdh$^{Q7/Q7}$ cells (Fig. 1 *C* and *D*). However, the percentage of apoptotic cells in STHdh$^{Q111/Q111}$ cells was dramatically reduced when *Sting* was knocked out (*Sting* KO) (Fig. 1 *C* and *D*). Similar results were also observed in *Cgas*-knockout (*Cgas* KO) STHdh$^{Q111/Q111}$ cells (Fig. 1 *C* and *D*). These results suggest that the cGAS–STING pathway is essential for mHTT-mediated apoptosis. To further verify these observations, we determined the levels of two apoptosis markers, cleaved caspases-3 and cleaved caspases-9 (47) in STHdh cells. The results showed that abundant

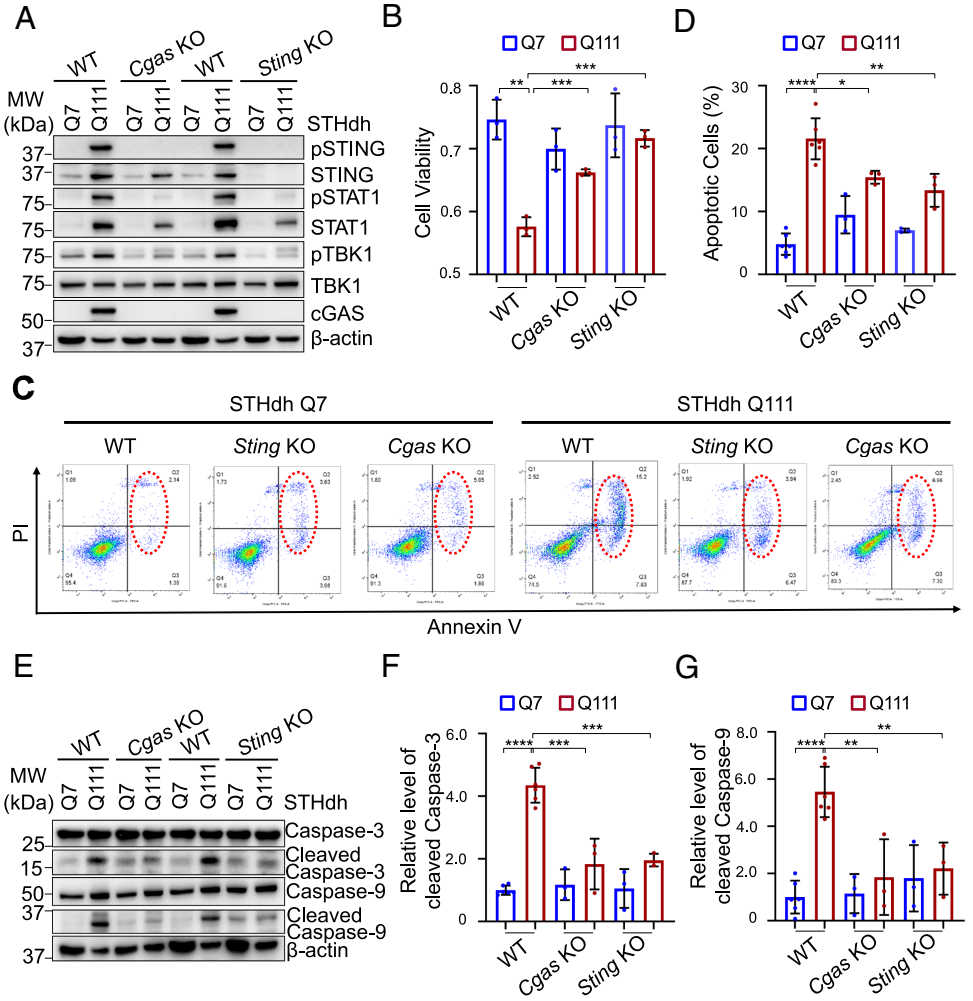

Fig. 1. mHTT-induced apoptosis depends on the cGAS–STING pathway. (*A*) Western blot analysis showing *Cgas*- and *Sting*-knockouts and inactivation of the cGAS–STING pathway in STHdh$^{Q7/Q7}$ (Q7) and STHdh$^{Q111/Q111}$ (Q111) cells. (*B*) MTS assays showing the inverse relationship between cell survival and cGAS/STING activity in mHTT cells. (*C*) Representative FACS scatter grams of the Annexin V apoptosis assay in *Cgas*- or *Sting*-knockout cells under 12 h-serum starvation. (*D*) Quantification of apoptotic cells by FACS analysis, as shown in *C*. (*E*) Western blot analysis showing inhibition of mHTT-induced apoptosis (indicated by the cleaved Capase-3 and cleaved Capase-9) by *Cgas*–*Sting* knockout. (*F* and *G*) Quantification of relative levels of cleaved Capase-3 (*F*) and cleaved Capase-9 (*G*). Statistical analyses were performed using two-tailed paired or unpaired *t* test or one-way ANOVA. When applied, data represent the mean ± SEM of three independent experiments. $^{*}P < 0.05$; $^{**}P < 0.01$; $^{***}P < 0.001$.

levels of cleaved caspases-3 and cleaved caspases-9 were observed in WT STHdh$^{Q111/Q111}$ cells but not in *Sting* KO cells nor in *Cgas* KO cells (Fig. 1 *E*–*G*). Taken together, the data shown here suggest that mHTT-mediated apoptosis is a cGAS–STING pathway-dependent event.

Cells Expressing mHTT Exhibit DNA Breaks and Accumulate Cytosolic DNA. Activation of the cytosolic DNA sensor cGAS relies on DNA damage-induced cytosolic DNA (17). To determine whether this is the case for mHTT-triggered cGAS activation, we first measured the level of γH2AX, a marker of DNA double-strand breaks (DSBs), in both HTT and mHTT cells. As shown in Fig. 2*A*, STHdh$^{Q111/Q111}$ cells exhibited a higher level of γH2AX than STHdh$^{Q7/Q7}$ cells. Higher levels of γH2AX were also observed in human HD fibroblast and mouse Raw264.7 macrophage cells expressing a 73-polyglutamine (73Q) mHTT–exon1 but not WT fibroblast and Raw264.7 cells expressing 23Q HTT–exon1 (*SI Appendix*, Fig. S1 *A* and *B*). We then detected cytosolic genomic DNA in the cytosolic fraction by real-time PCR using primers specific to the telomerase reverse transcriptase (*Tert*) gene (48). The amount of cytosolic genomic DNA in STHdh$^{Q111/Q111}$ cells was significantly higher than that in STHdh$^{Q7/Q7}$ cells (Fig. 2*B*). To further confirm the presence of cytosolic DNA in STHdh$^{Q111/Q111}$ cells, we directly visualized cytosolic DNA using an anti-dsDNA antibody as described (49, 50). Indeed, cytosolic dsDNA was observed in STHdh$^{Q111/Q111}$ cells, but not in STHdh$^{Q7/Q7}$ cells (Fig. 2 *C* and *D*). These data clearly show that cells expressing mHTT display DSBs and accumulate cytosolic DNA, which can be recognized by cGAS to activate the cGAS–STING pathway.

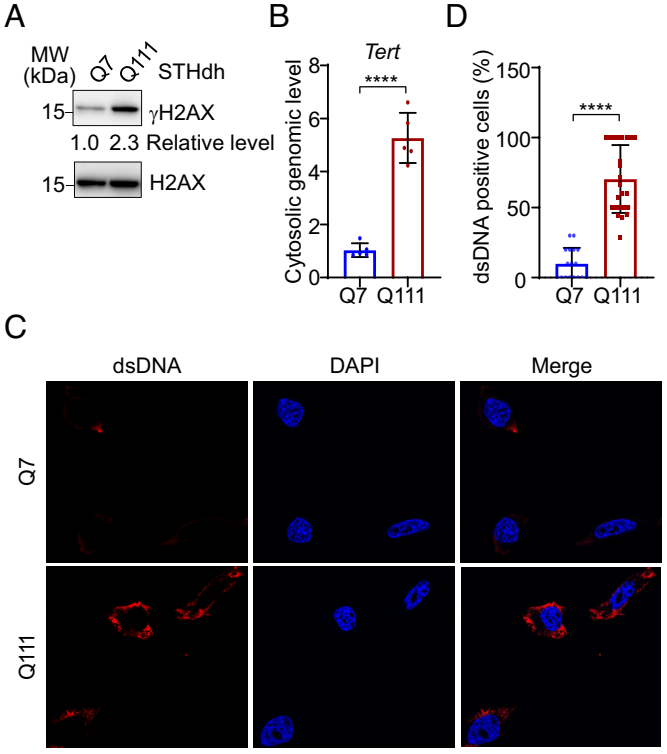

Fig. 2. HD cells display DSBs and accumulate cytosolic DNA. (*A*) Western blot analysis showing upregulation of γH2AX in Q111 cells compared with Q7 cells. (*B*) qPCR analysis showing significantly increased levels of cytosolic genomic DNA (*Tert*) in Q111 cells in comparison with those in Q7 cells. (*C*) Detection of cytosolic dsDNA in Q111 cells, but not in Q7 cells, by an anti-dsDNA antibody. (*D*) Percentage of cells displaying cytosolic DNA. The data for HTT and mHTT were derived from a total of 111 and 119 cells, respectively. Each dot represents an independent analysis and is the percentage of cells displaying cytosolic DNA in a microscope field of view. A total of 17 HTT and 24 mHTT microscope fields of view was analyzed. Statistical analyses were performed using two-tailed paired or unpaired *t* test or one-way ANOVA. When applied, data represent the mean ± SEM of the 17 and 24 microscope fields of view for HTT and mHTT, respectively. $^{****}P < 0.0001$.

Exo1 Is Essential for Activation of the cGAS–STING Pathway and Apoptosis in HD Cells. DSBs can be repaired in an error-free manner depending on HR, and Exo1 is a major nuclease that carries out DNA end resection, an essential step of DSB repair by HR (28). We have recently shown that the Exo1 nuclease activity during DNA end resection is negatively regulated by MutLα (30). Cancer cells defective in the MLH1 subunit of MutLα undergo excessive DNA end resection by Exo1, which causes severe DNA damage leading to the accumulation of cytosolic DNA and activation of the cGAS–STING pathway (30). To determine whether Exo1 is involved in the generation of cytosolic DNA in HD cells, we knocked out *Exo1* in both STHdh$^{Q111/Q111}$ and STHdh$^{Q7/Q7}$ cells (*SI Appendix*, Fig. S1 *C* and *D*) and analyzed the cytosolic DNA and innate immune signaling. Depletion of *Exo1* in STHdh$^{Q111/Q111}$ cells substantially reduced the amount of cytosolic genomic DNA (Fig. 3*A*), and this is also associated with reduced levels of pTBK1, pSTAT1, and pSTING (Fig. 3*B*). Correspondingly, reduced expression of the interferon-stimulated gene 15 (*Isg15*) and proinflammatory chemokine *Ccl5* was observed in *Exo1*-depletion STHdh$^{Q111/Q111}$ cells, as compared with control STHdh$^{Q111/Q111}$ cells (Fig. 3 *C* and *D*). These results suggest that Exo1 is essential for the generation of cytosolic DNA and activation of the cGAS–STING pathway in mHTT cells.

Next, we determined the impact of *Exo1*-depletion on mHTT-induced apoptosis. Annexin V assay (see above) showed that in comparison with WT controls, *Exo1*-depleted STHdh$^{Q111/Q111}$ cells exhibited a dramatic decrease in apoptosis (Fig. 3 *E* and *F*). To confirm this result, we detected the levels of cleaved caspase-3 and cleaved caspase-9 in WT and *Exo1*-depleted STHdh$^{Q111/Q111}$ cells and showed that the *Exo1*-depleted cells displayed significantly reduced levels of cleaved caspase-3 and cleaved caspase-9 (Fig. 3 *G*–*I*). These observations strongly suggest that Exo1 is essential for mHTT-mediated cytosolic DNA accumulation, cGAS–STING pathway activation, and apoptosis in HD cells.

To explore whether Exo1 functions in non-divided HD neuron cell, we established neuron-like cells from striatal precursors STHdh$^{Q111/Q111}$ and STHdh$^{Q7/Q7}$ cells using a well-established method (41). The resulting cells indeed exhibited neuron-like features including long neurites and the expression of MAP2 (microtubule-associated protein 2), a marker of maturing post-mitotic neuron (51) (*SI Appendix*, Fig. S2*A*). We found that STHdh$^{Q111/Q111}$ neuron-like cells displayed elevated levels of pSTING, pSTAT1, pTBK1, and apoptosis, i.e., increased cleaved caspases-3 and cleaved caspases-9. However, these phenomena were not observed in the similarly established neuron-like cells depleted of *Sting* or *Cgas* (*SI Appendix*, Fig. S2 *B*–*D*). Likewise, *Exo1*-depleted neuron-like cells showed characteristics of *Sting*-KO or *Cgas*-KO neuron-like cells (*SI Appendix*, Fig. S2 *B*–*D*), as well as those of *Exo1*-depleted STHdh$^{Q111/Q111}$ cells (compare Fig. 3 *G*–*I* with *SI Appendix*, Fig. S2 *B*–*D*). Taken together, these results suggest that mHTT induces apoptosis in both dividing and post-mitotic neuron-like cells in a manner dependent on Exo1 and the activation of the cGAS–STING pathway.

HTT Interacts with Exo1 and Negatively Regulates Exo1's Nuclease Activity. The involvement of Exo1 in mHTT-mediated apoptosis prompted us to hypothesize that HTT and mHTT differentially modulate Exo1's nuclease activity. To explore this possibility, we co-expressed the GFP–Exo1 and HTT–23Q–Myc,

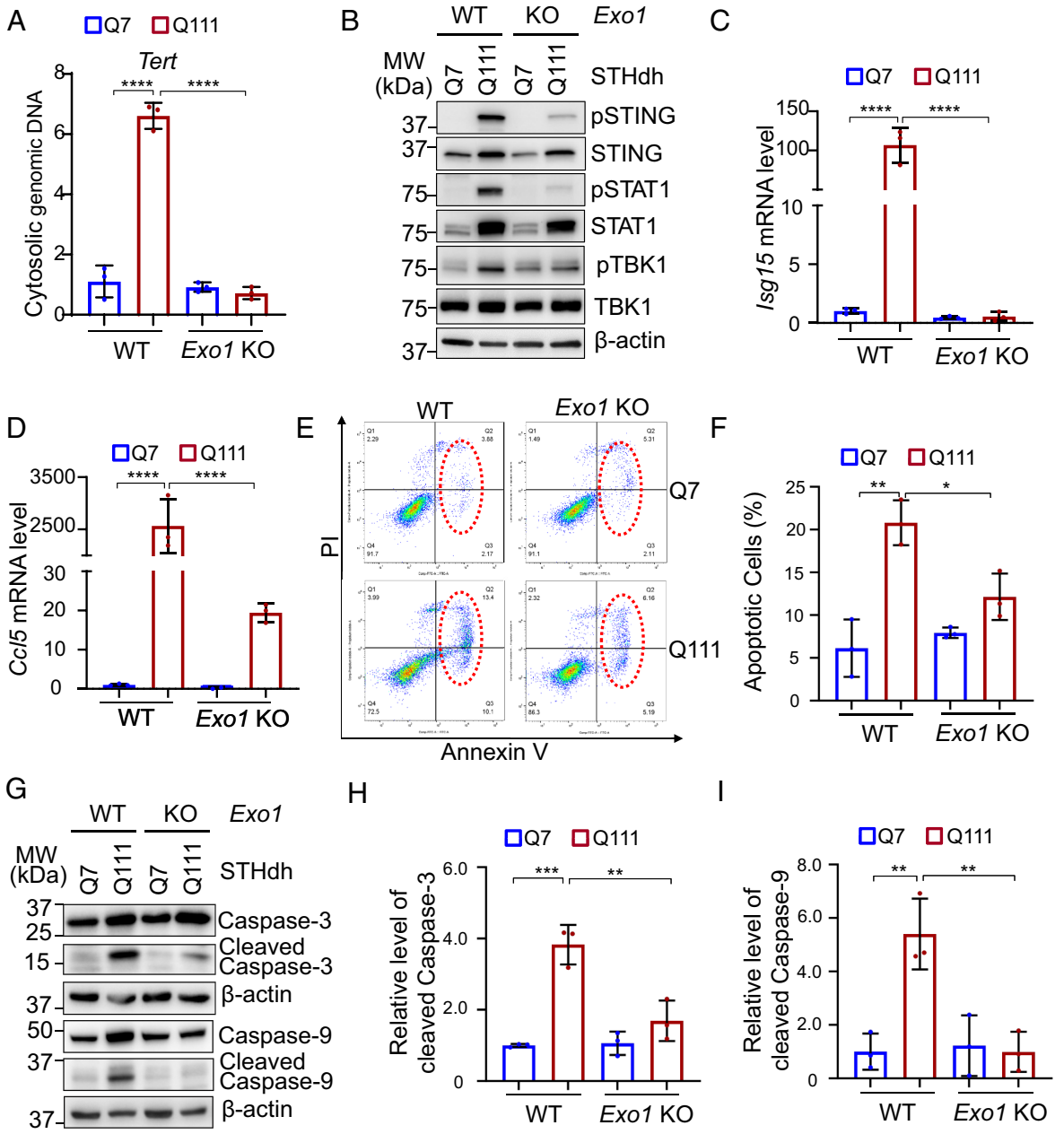

Fig. 3. Exo1 is essential for the cGAS pathway-mediated apoptosis in HD cells. (*A*) qPCR analysis that shows significantly reduced levels of cytosolic DNA in Q111 cells when Exo1 is depleted. (*B*) Western blots showing inactivation of the cGAS–STING pathway in Q111 cells when Exo1 is depleted. (*C* and *D*) qPCR analysis showing significantly reduced levels of *Isg15* (*C*) and *Ccl5* (*D*) in Q111 cells when Exo1 is depleted. (*E*) Representative FACS scatter grams of the Annexin V apoptosis assay in *Exo1*-depleted cells after 12 h serum starvation. (*F*) Quantification of apoptotic cells, as shown in *E*. (*G*) Western blots showing reduced levels of the cleaved Caspase-3 and cleaved Caspase-9, i.e., inhibition of apoptosis, in Q111 cells upon *Exo1* depletion. (*H* and *I*) Quantification of relative levels of cleaved Caspase-3 (*H*) and cleaved Caspase-9 (*I*) in *Exo1*-depleted cells. Statistical analyses were performed using two-tailed paired or unpaired *t* test or one-way ANOVA. When applied, data represent the mean ± SEM of three independent experiments. $^{*}P < 0.05$; $^{**}P < 0.01$; $^{***}P < 0.001$; and $^{****}P < 0.0001$.

mHTT–73Q–Myc fusion proteins in HEK 293 cells and performed co-immunoprecipitation (Co-IP) assays to determine physical interactions between Exo1 and HTT or mHTT. The results revealed that HTT–23Q pulled down significantly more GFP-Exo1 than mHTT (Fig. 4*A*), suggesting that mHTT possesses a significantly reduced Exo1-interacting activity. This result was further confirmed by the proximity ligation assay (PLA) in HEK 293 cells expressing HTT–23Q–Myc or mHTT–73Q–Myc, as cells with HTT–23Q–Myc showed more PLA signals than those with mHTT–73Q–Myc (Fig. 4*B*). To rule out the possibility that the aggregation of mHTT disrupts its interaction with Exo1, we expressed a known HTT/mHTT-interacting protein HAP40 (Huntington-associated protein 40) (52) in STHdh$^{Q7/Q7}$ and STHdh$^{Q111/Q111}$ cells and determined Flag-HAP40's interaction with HTT and mHTT in cell lysates by Co-IP assays. As shown in Fig. 4*C*, an HTT antibody pulled down similar amounts of Flag-HAP40 in STHdh$^{Q7/Q7}$ and STHdh$^{Q111/Q111}$ cell lysates, indicating that the reduced mHTT–Exo1 interaction observed in Fig. 4 *A* and *B* is not due to mHTT's aggregation. More convincingly, Exo1 was co-precipitated in STHdh$^{Q7/Q7}$, but not STHdh$^{Q111/Q111}$ lysates in the same Co-IP assay (Fig. 4*C*). Consistently, Co-IP assay using purified proteins also showed that a slightly more HAP40 was co-precipitated in the mHTT–48Q-containing reaction than in HTT–23Q-containing one, but the former reaction recovered much less Exo1 than in the latter one (*SI Appendix*, Fig. S3 *B* and *C*). Taken together, these results

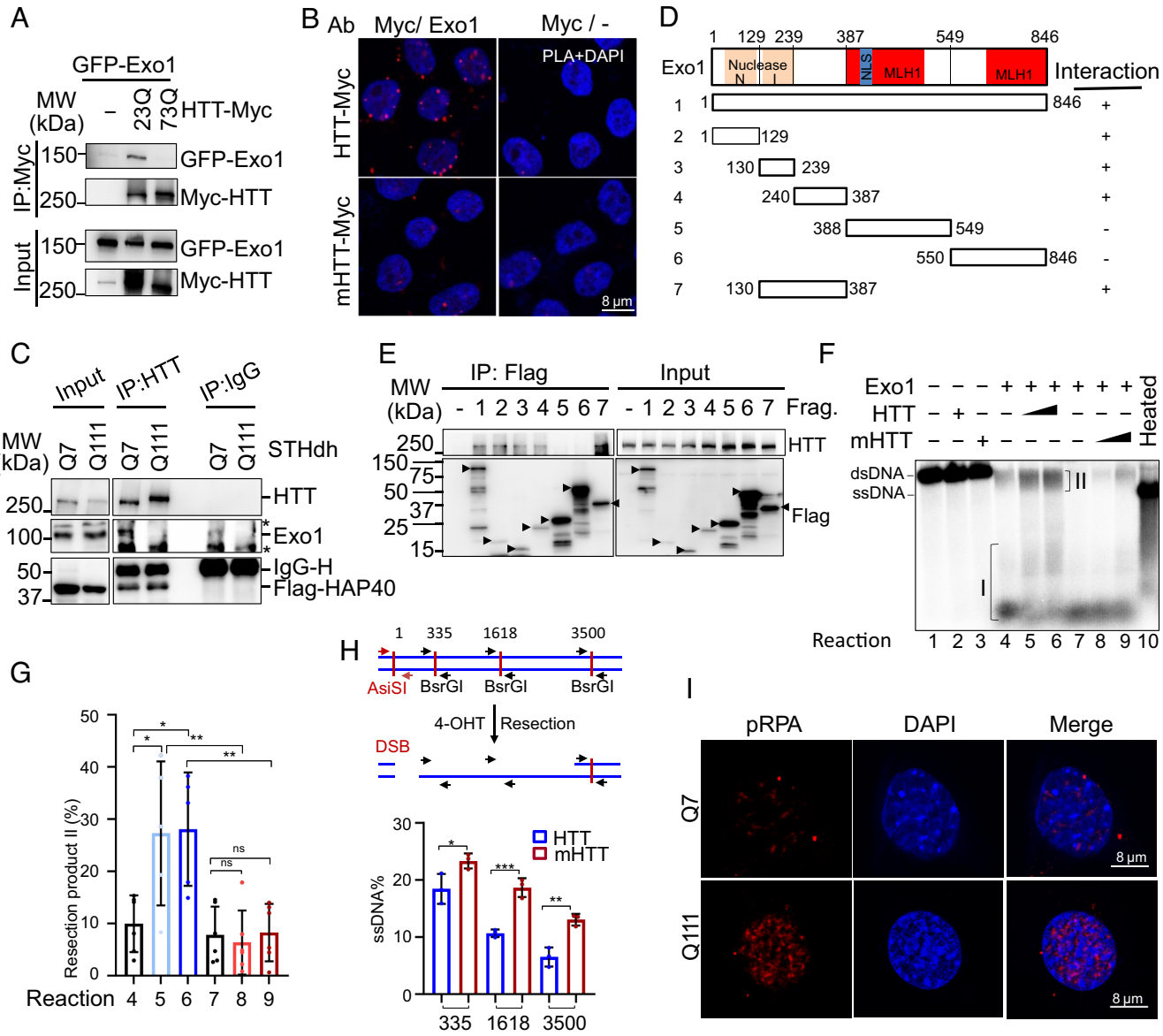

Fig. 4. HTT regulates Exo1's nuclease activity. (*A*) Co-immunoprecipitation-Western blotting analysis to show Exo1's physical interaction with HTT–23Q, but not mHTT–73Q in cell lysates derived from HEK293 cells, where Exo1 and HTT/mHTT were expressed as GFP and Myc fusion proteins, respectively. (*B*) PLA analysis showing differential interaction of Exo1 with HTT and mHTT. HTT–23Q–Myc or mHTT–73Q–Myc was expressed in HEK293 cells. Red fluorescence indicates positive PLA signals, suggestive of protein–protein interactions. Nuclei were stained with DAPI. (*C*) Co-IP-Western analysis showing that Exo1 interacts with HTT–Q7 but not mHTT–Q111 in STHdh cells. Flag-HAP40, a well-known factor that interacts with both HTT and mHTT, was expressed in Q7 and Q111 cells. One µg of cell lysate was used for Co-IP with an HTT antibody. Sign * represents non-specific bands. (*D*) Summary of PLA interactions of various Exo1 fragments with HTT. (*E*) Co-IP-Western analysis showing HTT's interactions with various Exo1 fragments, as indicated in *D*. Exo1 and its fragments were Flag-tagged at the N terminus and co-expressed separately with HTT in HEK293 cells. The individual cell lysates (1 mg) were incubated with M2 anti-Flag affinity beads. The beads-bound complexes were eluted by a 3xFlag peptide, recovered in the supernatant upon centrifugation, and analyzed by Western blotting using a HTT antibody (*Top* panel) or a Flag antibody (*Bottom* panel). Arrows point to the correct sizes of the individual Flag-Exo1 fragments, and sign * represents non-specific bands. (*F*) In vitro end-resection assay showing negative regulation of Exo1 nuclease activity by HTT but not mHTT. DNA substrate used is a ^{32}P-labled linearized 2.7-kb pUC19 plasmid (18 ng). Exo1 concentrations used is 3.0 pmol. The HTT or mHTT concentrations used in titration are 0.5 pmol and 1 pmol. (*G*) Quantification of resection products II, as shown in *F*. (*H*) Percentage of ssDNA generated during in vivo DNA end resection at the unique DSB site, AsiSI, in Chromosome 1. *Top*, the principle of in vivo end resection assay. *Bottom*, qPCR analysis showing increased amount of ssDNA generated at DSB site (AsiSI) in U2OS cells expressing mHTT–exon1, compared with those expressing HTT–exon1. (*I*) Immunofluorescence confocal images showing increased pRPA foci in Q111 cells compared with those in Q7 cells. Statistical analyses were performed using two-tailed paired or unpaired *t* test or one-way ANOVA. When applied, data represents the mean ± SEM of at least three independent experiments. $^{*}P < 0.05$; $^{**}P < 0.01$; $^{***}P < 0.001$; and $^{****}P < 0.0001$.

suggest that the PolyQ-expanded mHTT has significantly reduced its ability to interact with Exo1.

To identify the Exo1 domains responsible for interacting with HTT, we constructed six Flag-tagged Exo1 fragments, i.e., nuclease domain-containing fragments 1–129, 130–239, 130–387, and 240–387; 388–549, and 550–849 (Fig. 4*D*). We then co-expressed the individual Exo1 fragments with HTT–23Q in HEK293 cells, followed by Co-IP Western analysis. HTT–23Q was found to be co-precipitated with Flag- Exo1, Flag-1–129, 130–239, 240–387, and 130–387 (Fig. 4*E*). These results were also confirmed by the proximity ligation assay (PLA) in HEK 293 cells expressing individual Flag-tagged Exo1 fragments, as cells with Flag-Exo1, Flag-1–129, 130–239, 240–387, and 130–387 showed more PLA signals than those with Flag-388–549, and 550–849 (*SI Appendix*, Fig. S3*D*), strongly suggesting that HTT physically interacts with the N-terminal nuclease domain (1–387) of Exo1.

To determine whether the interaction between HTT and Exo1 affects Exo1's nuclease activity during end resection, we first performed in vitro end resection assay using a linearized plasmid (2.7 kb) DNA substrate labelled with ^{32}P at its 3′ ends (30, 53), and purified Exo1, HTT–23Q, and mHTT–48Q (*SI Appendix*, Fig. S3*A*). As expected, Exo1 by itself digested the DNA substrate into short pieces (Fig. 4*F*, lane 4, product I). Addition of the 23Q-containing HTT protein into the reaction significantly reduced the amount of product I but increased the amount of product II (Fig. 4*F*, compare lane 4 with lanes 5 and 6), which is slightly smaller than the original substrate. However, substitution of HTT–23Q with mHTT–48Q failed to generate the same products, instead, the mHTT-containing reaction showed essentially the same products observed in the Exo1-only reaction (Fig. 4*F*, compare lane 4 with lanes 8 and 9). The amount of resection II products in the HTT-containing reactions is significantly higher than that in reactions containing mHTT (Fig. 4*G*). These results indicate that HTT, but not mHTT, negatively regulates Exo1's nuclease activity, likely through its physical interaction with Exo1's nuclease domain.

To determine the impact of HTT or mHTT on DNA end resection in vivo, we used the DSB-inducible ER-AsiSI U2OS cell model (Fig. 4 *H*, *Upper*), which specifically induces a DSB at the AsiSI site located in chromosome 1 upon treating cells with 4-hydroxytamoxifen (4-OHT) (54). We established ER-AsiSI U2OS cells stably expressing HTT–exon1–23Q or mHTT–exon1–73Q by lentivirus infection (*SI Appendix*, Fig. S3*E*). The resulting cells displayed the expected phenotype, that is, increased pSTAT1 was observed in cells expressing mHTT–exon1–73Q, but not in cells expressing HTT–exon1–23Q after 4-OHT treatment (*SI Appendix*, Fig. S3*F*). To determine the amount of ssDNA generated during end resection at the DSB site (the AsiSI site), we designed three pairs of PCR primers to amplify DNA sequences from the AsiSI site to three BsrGI sites after DNA was digested with BsrGI (Fig. 4 *H*, *Upper* panel). Since ssDNA resists restriction digestion, the amount and the length of ssDNA produced during end resection can be determined by using these three pairs of quantitative PCR (qPCR) primers. If DNA end resection is appropriately regulated, less amount of ssDNA is generated; otherwise, large amount of ssDNA is expected. The results showed that although the amount of ssDNA upon 4-OHT treatment was inversely correlated with the distance between the AsiSI and BsrGI sites in both HTT–exon1–23Q and mHTT–exon1–73Q cells, mHTT–exon1–73Q cells generated significantly higher levels of ssDNA at all three BsrGI sites than HTT–23Q cells (Fig. 4 *H*, *Lower* panel). Taken together, these results suggest that HTT negatively regulates DNA end resection, likely through its physical interaction with Exo1.

ssDNA binding protein RPA (replication protein A) protects ssDNA from nuclease digestion during DNA metabolism, and its phosphorylation serves as an indicator of DNA damage (55–57). Thus, the generation of a large quantity of ssDNA during DNA end resection in mHTT cells should be associated with an increased amount of phosphorylated RPA (pRPA) and increased pRPA foci. We analyzed pRPA in STHdh$^{Q7/Q7}$ and STHdh$^{Q111/Q111}$ cells and observed a significant increase in the pRPA foci number per cell (Fig. 4*I* and *SI Appendix*, Fig. S3*G*) and the percentage of pRPA-positive cells (*SI Appendix*, Fig. S3*H*) in STHdh$^{Q111/Q111}$ cells, as compared with STHdh$^{Q7/Q7}$ cells. Collectively, our in vitro and in vivo data strongly support the idea that HTT negatively regulates Exo1's nuclease activity during DNA repair, but mHTT has lost this function.

HTT Interacts with Mismatch Repair Factor MLH1. Since MutLα (MLH1–PMS2) functions to negatively regulate the Exo1-catalyzed DNA excision (30) and since MLH1 is an important genetic modifier of HD (32, 33), we hypothesized that HTT and mHTT may differentially regulate Exo1's nuclease activity via their interactions with MLH1. To explore this possibility, we first performed Co-IP analysis to determine whether HTT or mHTT physically interacts with MutLα using all purified proteins in the presence of Exo1. As expected, an MLH1-antibody efficiently pulled down Exo1 regardless of the presence of HTT or mHTT (Fig. 5*A*), confirming that MutLα interacts with Exo1 (30, 58). The antibody also co-precipitated significantly more amount of HTT–23Q than that of mHTT–48Q (Fig. 5 *A* and *B*), suggesting that the presence of the expanded polyQ residues in mHTT has significantly impeded mHTT's interaction with MLH1. To further determine the interactions between these proteins, we co-expressed GFP–Exo1, Flag–MLH1, and HTT–23Q–Myc or mHTT–73Q–Myc fusion proteins in HEK 293 cells and performed Co-IP assays using an antibody against Flag. The results showed that the pulldown level of HTT–Myc is significantly higher than that of mHTT–Myc (Fig. 5 *C* and *D*). Collectively, the data presented here suggest that mHTT interacts with MLH1 to a much lesser extent compared to HTT.

To determine the impact of the HTT–Exo1–MutLα ternary complex on Exo1's nuclease activity, we performed in vitro end resection assay. The results showed that MutLα or HTT alone could efficiently conquer the Exo1's nuclease activity during end resection, as the reaction containing both MutLα and HTT generated no additional amount of product II in comparison with those containing only MutLα or HTT (Fig. 5 *E* and *F*, reactions 5, 6 and 7). This suggests that HTT and MutLα can work together to suppress Exo1's activity, although they could act independently. We also found that replacing HTT with mHTT did not disrupt MutLα's ability to control Exo1's activity, as similar amounts of product II were produced in the Exo1-MutLα-containing reactions in the presence or absence of mHTT (Fig. 5 *E* and *F*, compare reactions 5 and 9). This finding raised the question of why HD cells with functional *MLH1* and *PMS2* genes display hyperactive DNA end resection.

MLH1 Exhibits a Shorter Half-life in mHTT Cells than in HTT Cells. To answer the aforementioned question, we analyzed MLH1 levels in whole cell lysates (WCL) and chromatin fractions derived from STHdh$^{Q7/Q7}$ and STHdh$^{Q111/Q111}$ cells. Surprisingly, both WCL and chromatin-bound MLH1 levels in STHdh$^{Q111/Q111}$ cells were significantly lower than those in STHdh$^{Q7/Q7}$ cells (Fig. 6 *A* and *B*). The MLH1 reduction in STHdh$^{Q111/Q111}$ cells was not due to gene expression, as the *MLH1* mRNA level in STHdh$^{Q111/Q111}$ was actually higher than that in STHdh$^{Q7/Q7}$ cells (Fig. 6*C*). We then analyzed the MLH1 level in the striatum tissues of HD knock-in mouse model Q175 (59). The results showed that HD mice express an MLH1 level significantly lower than that in WT animals (Fig. 6 *D* and *E*). The low MLH1 expression in HD mice is associated with high levels of γH2AX, pSTAT1 and cleaved caspase-9 (Fig. 6*D* and *SI Appendix*, Fig. S4 *A–C*), suggesting that striatum cells with low MLH1 expression in HD animals undergo mHTT-mediated cGAS–STING activation-trigged apoptosis. To further confirm that it is the MLH1 level that dictates the apoptotic event in mHTT cells, we overexpressed MLH1 in STHdh$^{Q111/Q111}$ cells and determined the status of the cGAS–STING activation and the cleavage of caspase-3 and caspase-9. As shown in *SI Appendix*, Fig. S5 *A–D*, overexpression of MLH1 in STHdh$^{Q111/Q111}$ cells greatly reduced the levels of pTBK1, pSTAT1, pSTING, as well as the levels of cleaved caspase-3 and cleaved caspase-9, suggesting inactivation of the cGAS–STING pathway and inhibition of apoptosis. These results prompted us to measure the stability of MLH1 in STHdh cells. We treated STHdh cells with the protein synthesis inhibitor cycloheximide

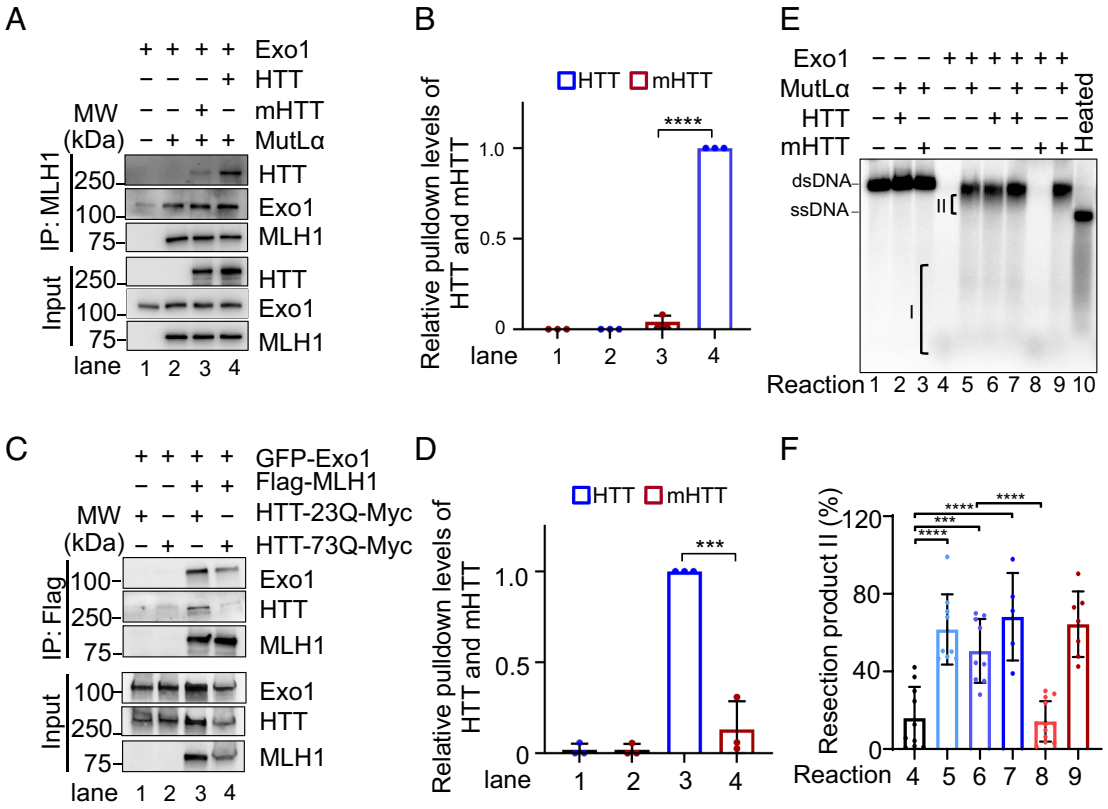

Fig. 5. Interactions between HTT, Exo1, and MLH1 regulate Exo1's nuclease activity. (*A*) Protein pulldown assays showing that the interactions of mHTT or HTT with Exo1 and MLH1 (MutLα) using purified proteins. (*B*) Quantification of the relative amount of HTT and mHTT in pulldown assay, as shown in *A*. (*C*) Co-IP Western analysis showing differential interactions of mHTT or HTT with Exo1 and MLH1 (MutLα). Flag–MLH1, GFP–Exo1, HTT–23Q–Myc, and mHTT–73Q–Myc fusion proteins were expressed in HEK293 cells. One mg of the cell lysates was used in Co-IP assay. (*D*) Quantification of relative amounts of the immunoprecipitated HTT and mHTT, as shown in *C*. (*E*) In vitro end-resection assays. DNA substrate used is a linearized 2.7-kb pUC19 plasmid (18 ng). Proteins concentrations used are 3.0 pmol Exo1, 0.5 pmol HTT or mHTT, and 0.5 pmol MutLα. (*F*) Quantification of the amount of resection product II, as shown in *E*. Statistical analyses were performed using two-tailed paired or unpaired *t* test or one-way ANOVA. When applied, data represents the mean ± SEM of at least three independent experiments. $^{*}P < 0.05$; $^{**}P < 0.01$; $^{***}P < 0.001$; and $^{****}P < 0.0001$.

(CHX) and found that MLH1 in STHdh$^{Q111/Q111}$ cells exhibited a half-life much shorter than that in STHdh$^{Q7/Q7}$ cells (Fig. 6 *F* and *G*). Because HTT, but not mHTT, interacts with MLH1 (Fig. 5 *A* and *C*), these results suggest that the HTT–MLH1 interaction plays an important role in stabilizing MLH1, which explains why cells expressing mHTT, but not those expressing HTT, accumulate cytosolic DNA to promote the activation of the cGAS–STING pathway and apoptosis.

Discussion

HTT is ubiquitously expressed across tissues. It has an interactome over 400 proteins, but its cellular functions are not clearly defined (60). The toxic mHTT protein is the pathogenic driver of HD by inducing pathological changes both in brain and peripheral system, such as blood, muscle, liver, and lung (61–63). However, the causing mechanism of the pathology is not fully understood. In this study, we find that HTT functions as an important regulator to constrain the hyperactive nuclease Exo1 during the repair of DSBs through protein–protein interactions, which prevents unnecessary digestion of genomic DNA. Conversely, mHTT no longer possesses this nuclease-regulating activity, thereby allowing Exo1 to catalyze uncontrolled DNA degradation, which eventually induces cytosolic DNA and triggers cGAS–STING-mediated apoptosis. Therefore, this study has identified unique functions for both HTT and mHTT, uncovering the molecular basis of mHTT-mediated cell death in HD.

Exo1 is an important 5′ to 3′ exonuclease required for multiple DNA repair pathways, including MMR and DSB repair, and the hyperactive nuclease activity of Exo1 is properly controlled by MutLα to avoid unnecessary DNA digestion. Exo1 catalyzes excessive excision during MMR and DNA end resection in the absence of MutLα, which leads to chromosome instability and generation of cytosolic DNA to activate the cGAS–STING pathway (30). These phenomena disappear when MutLα is restored or Exo1 is depleted in cells. MutLα executes its regulatory function via its physical interaction with Exo1 (30). We show here that like MutLα, HTT negatively regulates Exo1's nuclease activity by interacting with Exo1. Interestingly, we also found that these two Exo1 regulatory proteins interact with each other, suggesting the formation of an HTT–Exo1–MutLα ternary complex, which provides a dual regulatory mechanism to properly constrain Exo1's nuclease activity.

However, the conversion of HTT to mHTT has largely destroyed this dual control mechanism. First, mHTT barely interacts with Exo1, thereby failing to regulate Exo1 during DNA repair. Second, unlike HTT, which interacts with and stabilize MutLα, mHTT has essentially lost its ability to interact with MutLα. This is likely the reason that the MLH1 subunit of MutLα displays a much shorter half-life in cells expressing mHTT than in those expressing HTT (Fig. 6*F*). This also explains why HD cells accumulate cytosolic DNA, because they have lost the Exo1's primary regulator in MutLα, leading to uncontrolled end resection, which in turn causes severe DNA and chromosome damage to

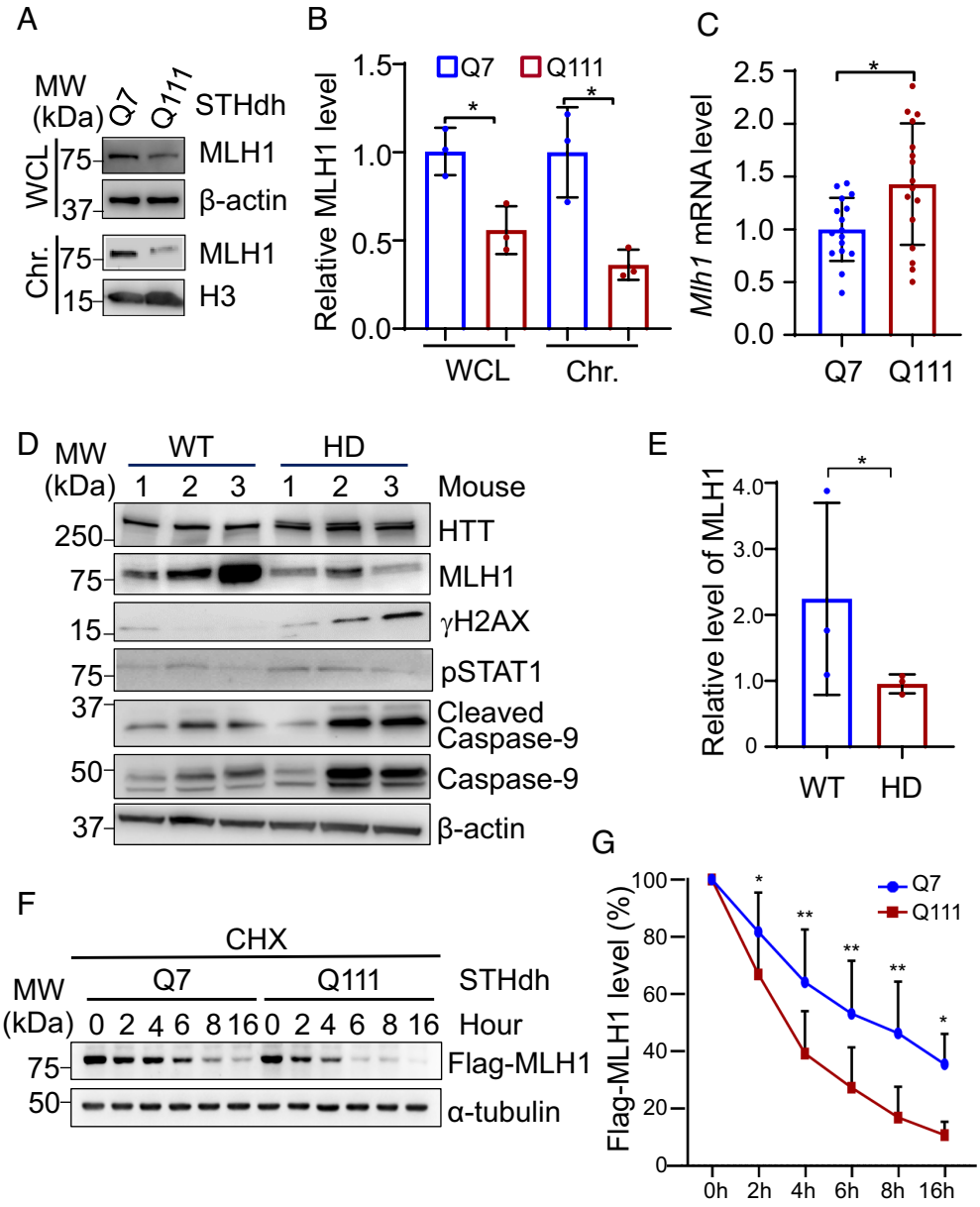

Fig. 6. MLH1 is unstable in HD. (*A*) Western blot analysis showing decreased MLH1 protein levels in the whole cell lysate (WCL) and chromatin fraction (Chr.) of STHdh$^{Q111/Q111}$ (Q111) cells compared with STHdh$^{Q7/Q7}$ (Q7) cells. (*B*) Quantification of the relative MLH1 protein level in Q7 and Q111 cells. (*C*) qPCR analysis showing the levels of *Mlh1* mRNA in Q7 and Q111 cells. (*D*) Western blot analysis showing the expression levels of MLH1 (reduced), γH2AX (increased), pSTAT1 (increased) in Q175 HD mouse striatum. (*E*) Quantification of the amount of MLH1 protein level as shown in *D*. (*F*) Western blotting analysis showing the half-life of Flag-MLH1 in Q7 and Q111 cells in the presence of 100 μg/mL cycloheximide (CHX). (*G*) Quantification of the relative levels of the Flag-MLH1 protein in Q7 and Q111 cells, as shown in *G*. Statistical analyses were performed using two-tailed paired or unpaired *t* test or one-way ANOVA. When applied, data represents the mean ± SEM of three independent experiments. $^{*}P < 0.05$; $^{**}P < 0.01$; $^{***}P < 0.001$; and $^{****}P < 0.0001$.

release damaged DNA to the cytoplasm (30). Recently, Roy et al. have shown that the endonuclease domain of MLH3, a subunit of MutLγ (MLH1–MLH3) promotes CAG expansion in HD animal models, as disrupting or mutating the MLH3 endonuclease motif eliminates the *HTT* CAG expansion (64). This suggests that the MutLγ endonuclease activity facilitates CAG repeat expansion and the production of mHTT. Notably, a functional MutLα (MLH1–PMS2), the major MutL heterodimer in mammalian cells (29, 65) and the initial MutL homologs identified to possess an endonuclease activity (66), is present in the Roy et al. study (64). It remains to be determined why the MutLα endonuclease activity does not contribute to the *HTT* CAG expansion in the HD model (64). Nevertheless, the findings in this study and ours suggest that the molecular interplays between MutLα/MutLγ and HTT/mHTT controls HD onset and progression. Further investigations are required to elucidate the basis of these interactions.

In addition to its interaction with mismatch repair proteins, HTT has also been shown to be involved in other DNA repair pathways, including transcription-coupled nucleotide excision repair, non-homologous end joining of DSB repair and ATM signaling (20–25). Despite that HR and NHEJ are mainly responsible for DSB repair in dividing neural stem/progenitor cells and post-mitotic neurons, respectively (67), both sub-pathways are active in mature neurons (68). How HR occurs in mature neurons without dividing cells remains to be investigated. Further studies are also required to determine mHTT's roles not only in neurons but also in other types of cells such as astrocytes and blood cells (9, 69).

Based on the published data and the results presented here, we propose a working model (Fig. 7) to elucidate the mechanism by

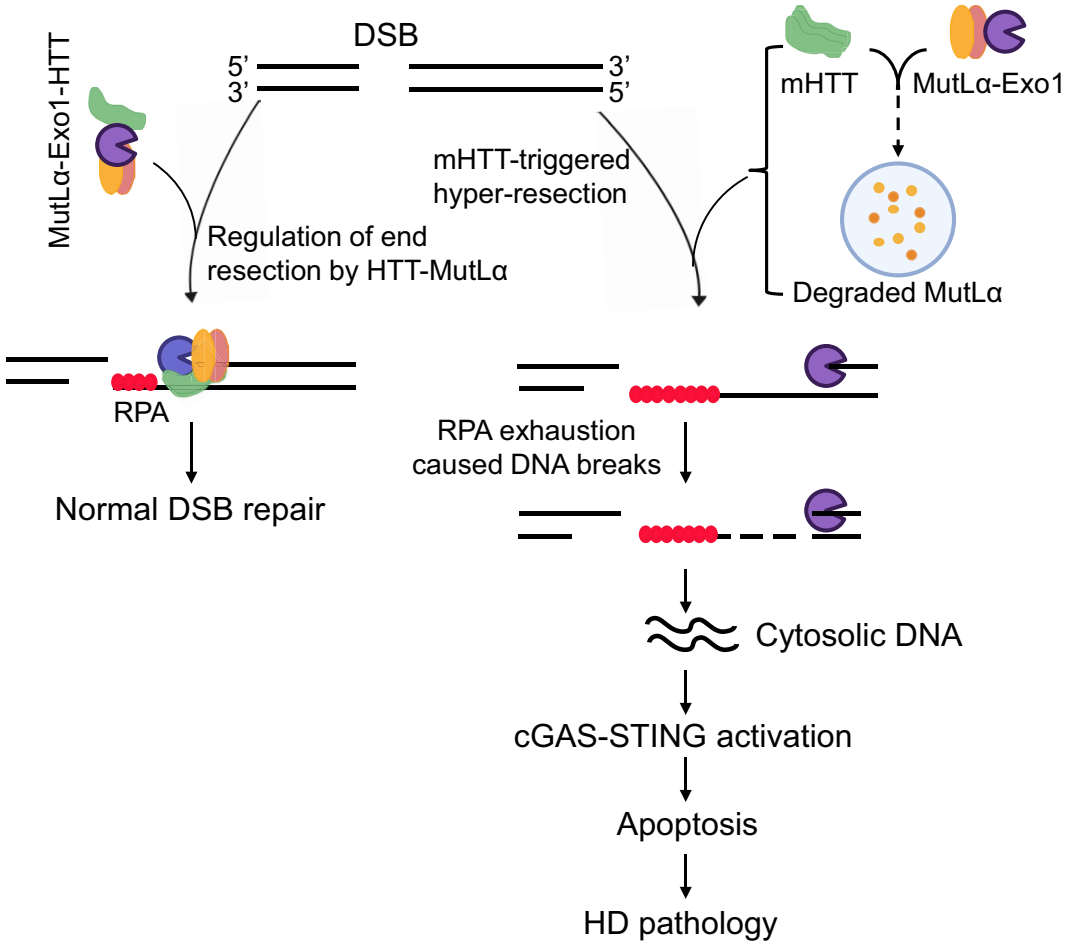

Fig. 7. Model for mHTT-triggered cGAS-dependent apoptosis. Under normal conditions, HTT forms a ternary complex with MutLα and Exo1, which properly terminates Exo1-catalyzed end resection, resulting in normal DSB repair via homologous recombination (*Left*). However, in HD cells, mHTT barely interacts with Exo1 nor MutLα. Rather, mHTT promotes degradation of the Exo1 primary regulator MutLα, leading to an uncontrolled DNA end resection (*Right*). The hyperactive Exo1 generates a large quantity of ssDNA to exhaust the pool of RPA, and the unprotected ssDNA can be readily digested by various nucleases. This causes severe DNA damage and produces cytosolic DNA to activate the cGAS–STING pathway, thereby promoting apoptosis in HD.

which HTT or mHTT distinctly regulates Exo1's nuclease activity during DNA end resection, leading to normal DNA repair or severe DNA damage that induces apoptosis, respectively. In WT HTT cells, DNA end resection by Exo1 is properly terminated by the protein–protein interactions between HTT, MutLα, and Exo1, so that DSB repair by HR occurs normally (Fig. 7, *Left*). However, in HD cells, although both normal HTT and mHTT are expressed, mHTT functions dominantly over HTT. Therefore, the presence of mHTT has largely destroyed the HTT–Exo1 and HTT–MutLα interactions, with the former interaction directly suppressing Exo1's nuclease activity, and the latter one facilitating the stability of MutLα. Thus, in the presence of mHTT, MutLα undergoes rapid degradation, which renders HD cells lose the primary Exo1's regulator. The hyperactive Exo1 generates a large quantity of ssDNA to exhaust the pool of RPA, leaving the extra ssDNA unprotected. The unprotected ssDNA can be readily digested by various nucleases, resulting in abnormal HR and other aberrations (30). This generates cytosolic DNA to activate the cGAS–STING pathway, thereby promoting cell death in HD (Fig. 7, *Right*).

The data described here provide potential targets for treating HD. Since mHTT-mediated apoptosis depends on an active cGAS–STING pathway, factors that block cGAS activation and its downstream signaling could inhibit mHTT-induced apoptosis. Insights into the structural and molecular biology of the cGAS–STING pathway have paved the way for developing small-molecule inhibitors to target the cGAS–STING components in a number of human diseases (70). These small-molecule inhibitors could be good candidates for treating HD patients. Given that mHTT differs from HTT by the expanded polyQ, the expanded polyQ could be the toxic activity responsible for inhibiting its interaction with MLH1. If this is true, identifying factors that specifically inhibit the polyQ activity could benefit HD patients. Future studies will address these potential clinical applications.

Because the apoptosis we observed in HD-derived cells is dependent on Exo1-catalyzed hyper-end resection, questions raised from this concern whether or not the repair of DSBs in HD cells is through HR, which usually occurs in the S and G2 phases of the cell cycle, but not in post-mitotic cells such neuron cells, whether or not the uncontrolled Exo1 nuclease activity in HD cells is associated with HR, and whether or not the observed phenomenon is relevant to neuronal cell death. Although it is difficult to answer all these questions, we do find that neuron-like cells expressing mHTT display elevated apoptotic signals and activated cGAS–STING pathway, but these phenomena all disappeared in *Exo1*-depleted neuron-like cells (*SI Appendix*, Fig. S2). These results strongly suggest that Exo1 indeed mediates mHTT-triggered, cGAS pathway-dependent apoptosis in neuron-like and post-mitotic cells.

In fact, DSB repair via HR has been reported in mature neurons (68). Although how it occurs is not fully understood, transcription-coupled nucleotide excision repair (TC-NER), which is active in neurons, has been postulated to stimulate HR in post-mitotic cells (71). In this case, stalling of RNA polymerase II (Pol II) at the damage site

recruits CSB to initiate TC-NER. The lesion processing by TC-NER provides a platform to recruit HR factors such as Rad52 and Rad51C via their physical interaction with CSB. This recruitment allows the Pol II–CSB initiation complex to switch TC-NER to TC-HR, which could be an important way to ensure the stability of Pol II-transcribed genes, particularly for neurons with long-term viability. However, this speculation requires thorough investigations.

It is also possible that the MMR-mediated DNA damage response (72) is involved in mHTT-triggered apoptosis. This pathway, which does not require DNA replication and cell division but Exo1 and MutSα, is activated when MutSα binds to a non-mismatched DNA lesion such as a UV-dimer (73) or chemically modified adduct (74, 75). The activation of the MMR-mediated damage response induces a futile repair cycle (76), leading to apoptosis (72, 75). Future studies are required to make this connection.

Experimental Materials and Methods

Cell Lines and Culture Conditions. Unless otherwise mentioned, cells used in this study were purchased from the Coriell Institute for Medical Research, and all cells were maintained at 37 °C in a humidified 5% CO_2 incubator. STHdh$^{Q7/Q7}$ (Q7) and STHdh$^{Q111/Q111}$ (Q111) mouse striatal cell lines that express full-length wild-type (polyQ7) and mutant (polyQ111) HTT were cultured in Dulbecco's modified Eagle's medium (DMEM) with high glucose, 10% fetal bovine serum (FBS), 1% penicillin-streptomycin, and 40 μg/mL G418 at 33 °C (41). To establish neuron-like cells, we cultured STHdh$^{Q7/Q7}$ or STHdh$^{Q111/Q111}$ cells in serum-free DMEM medium containing 10 ng/mL aFGF, 250 μM IBMX, 200 nM PMA, 50 μM forskolin, and 5 μM dopamine for 16 h, as described (41). To knock out *Sting* or *Cgas*, we transfected STHdh$^{Q7/Q7}$ and STHdh$^{Q111/Q111}$ cells with CRISPR/Cas9 system plasmid pX458-g*Sting*, pX458-g*Cgas* or control in a 6-cm dish. GFP-expressing cells were individually seeded in a 96-well plate to establish single clones, and *Sting* or *Cgas* depletion was confirmed by Western blotting using a STING or cGAS antibody. *Exo1* knockout was similarly performed using the CRISPR-Cas9 technology, and the knockout was confirmed by qPCR analysis of *exo1* mRNA (*SI Appendix*, Fig. S1*C*). Raw264.7 cells, which were cultured in a RPMI 1640 medium supplemented with 2 mM L-glutamine and 10% FBS and 1% penicillin-streptomycin, were used to stably express Flag-tagged HTT exon 1 with 23Q (Flag–HTT–exon1-23Q) or 73Q (Flag–HTT–exon1–73Q) by transducing lentiviral particles carrying the genes expressing these fusion proteins. Human fibroblast cells (GM02153, GM21756) were cultured in Eagle's Minimum Essential Medium with Earle's salts, non-essential amino acids, 15% FBS, and 1% penicillin-streptomycin.

Confocal Immunofluorescence Analysis. Cells were cultured on glass coverslips fixed with 4% paraformaldehyde in PBS. After extensive washing with PBS, cells were permeabilized with Triton X-100 (0.2% in PBS), blocked with 5% BSA in PBS, and incubated with primary antibodies (diluted in 2% BSA) at 4 °C overnight. Cells were then washed with PBS, incubated with appropriate secondary antibodies (1:1,000 in PBS) at room temperature for 1 h, followed by washing mounting with ProLong™ Diamond Antifade Mountant with DAPI (ThermoFisher Scientific, Cat# P36961). Cell images were captured using a Leica TCS SP8 confocal microscope.

Cell Lysate Preparation and Western Blot Analysis. Whole-cell lysates (WCL) were prepared by radioimmunoprecipitation assay (RIPA) buffer [150 mM NaCl, 0.5% sodium deoxycholate, 0.1% SDS, 1% NP-40 dissolved in 50 mM Tris (pH 8.0)]. Separation of cytoplasmic and chromatin fractions was prepared as described (77). Briefly, cells were resuspended in the lysis buffer (10 mM HEPES, pH 7.4, 10 mM KCl, 0.05% NP-40, protease inhibitors) for 20 min on ice. Samples were centrifuged at 14,000 rpm for 10 min, and the supernatants were collected as cytosolic extracts. The pellets were washed with the lysis buffer and centrifuged at 14,000 rpm for 5 min, and the resulting pellets were resuspended in 0.2 N HCl and incubated on ice for 10 min before centrifugation. The supernatants were then neutralized with 1.0 M Tris buffer (pH 8.5) and collected as chromatin fractions. Proteins in WCL and chromatin fractions were resolved by SDS-PAGE, transferred onto nitrocellulose membrane, and subjected to Western blotting analysis using the indicated antibodies. The protein band intensities were quantified with ImageJ software (NIH) and normalized against β-actin.

Co-immunoprecipitation and In Vitro Pull-down Assay. Cultured cells (1×10^7 cells) were lysed in buffer containing 20 mM Tris (pH 7.4), 150 mM NaCl, 1 mM EDTA, 1 mM EGTA, 1% Triton X-100, benzonase nuclease and protease inhibitors for 30 min on ice and then centrifuged for 15 min at 14,000 rpm at 4 °C. Unless mentioned otherwise, 500 μL lysates (1 μg/μL) were precleared for 1 h with protein G beads. The precleared supernatant was incubated overnight with 1 μg of antibodies, as indicated. The immune complex was then precipitated by incubation with protein G bead (GE Healthcare Life Sciences, Cat#28-9440-08) for 2 h at 4 °C. Immunoprecipitants, or whole-cell extracts (WCEs) were analyzed by the standard Western blotting.

For pulldown experiments, 1 μg of the indicated proteins and 1 μg antibody were incubated in buffer A (20 mM Tris pH 7.4, 100 mM NaCl, 1 mM EDTA, 1% Triton X-100 and protease inhibitors) for 2 h and subjected to immunoprecipitation after incubation with protein G beads (GE Healthcare Life Sciences, Cat#28-9440-08) for 1 h at 4 °C. Immunoprecipitants or input proteins were analyzed by the standard Western blotting. Purified HTT/mHTT proteins are purchased from Coriell Institute. Recombinant Exo1 and MutLα proteins were expressed in insect cells and purified, as described (78). Purified Flag-HAP40 protein was expressed in HEK293 cells and purified with M2 anti-Flag affinity beads (Millipore Sigma, Cat#A2220) and 3× Flag peptide (Millipore Sigma, Cat#F4799) elution.

Proximity Ligation Assay (PLA). Cells were plated on glass coverslips and cultured in DMEM for 24 h before being transfected with the indicated plasmids. Forty-eight hours after transfection, cells were fixed with 4% paraformaldehyde, permeabilized with 0.5% Triton-X100, washed with PBS, and incubated with the primary antibodies, as indicated. Samples were subjected to PLA assays using the Duolink PLA kit (Millipore). Nuclei were stained with DAPI (ThermoFisher Scientific, Cat# P36961). Cell images were captured using a Leica TCS SP8 confocal microscope.

Cell Viability Assay. Cell viability assay was carried out to assess the percentage of viable cells using the CellTiter 96 MTS Aqueous One solution cell proliferation assay (Promega). In brief, wide type, *Sting* or *Cgas* knockout STHdh$^{Q7/Q7}$ and STHdh$^{Q111/Q111}$ cells were seeded at 3,000 cells/well in a 96-well plate. After incubation in normal culture medium for 72 h, cells were cultured in the medium containing 20% MTS for 2 h before measuring the absorbance (OD) at 490 nm. All experiments were repeated three times with each time point set up with four replicates.

RNA Extraction and Real-Time PCR Analysis. All RNA was isolated using the TRIzol™ Reagent kit (Invitrogen, Cat# 15596026). cDNA was synthesized from 1 μg of RNA using Reverse Transcription Supermix (BioRad, Cat#1708840), and

used to detect the expression levels of multiple genes by quantitative RT-PCR (qRT-PCR) using gene-specific primer sets (*SI Appendix*, Table S1) and SsoAdvanced™ Universal SYBR Green Supermix, according to the manufacturer's instructions (Biorad, Cat#1725271). The gene expression levels were normalized using GAPDH as a control. The $2^{-\Delta\Delta Ct}$ method was used to calculate relative expression changes.

Extraction and Quantification of Cytosolic DNA. Cytosolic DNA was isolated following a previously published protocol (79). Cultured cells (2×10^7) were divided into two equal aliquots and one aliquot was resuspended in 500 µL of NaOH (50 µM), boiled for 15 min, and then neutralized with 50 µL of 1 M Tris-HCl (pH 8.0). The resulting sample served as normalization controls for the total amount of DNA. The other aliquot was resuspended in 500 µL of permeabilization buffer (50 mM HEPES, pH 7.4, 150 mM NaCl, 2 mM EDTA, and 25 µg/mL digitonin). Cells were centrifuged at 1,000*g* for 3 min, and the supernatant was transferred to a fresh tube and centrifuged at 17,000*g* for 10 min to remove mitochondria contamination, with the end sample being regarded as cytosolic DNA. Both samples were treated with protease K and purified using DNA Clean & Concentrator (ZYMO RESEARCH). Real-time PCR was performed to detect genomic DNA (gDNA) by genomic DNA primers (*Tert*). Cytosolic gDNA levels were normalized with total gDNA.

Annexin V and Flow Cytometry Analyses. Cells were collected after 12 h of serum starvation and stained with annexin V or annexin V and propidium iodide (PI) as indicated using FITC Annexin V Apoptosis Detection Kit I (Cell Signaling) according to the manufacturer's instructions. FACS analysis was performed using a FACS lyric flow cytometer and FlowJo software (BD Biosciences).

In Vitro and In Vivo DNA End Resection Assays. In vitro and in vivo DNA end resection assays were performed as described previously (30). The in vitro assays were assembled in 20-µL reactions containing 18 ng of 3′-end ^{32}P-labeled linearized pUC19 plasmid DNA (2.7 kb), the indicated proteins, 25 mM MOPS (pH 7.0), 2 mM DTT, 60 mM KCl, 1% Tween 20, 2 mM ATP, 5 mM $MgCl_2$. Unless mentioned otherwise, the protein concentrations used in the experiments are 3 pmol Exo1, 0.5 pmol HTT, 0.5 pmol mHTT, and 0.5 pmol MutLα. Reactions were incubated at 37°C for 30 min and terminated with 5 µL of Proteinase K buffer (2% SDS, 150 mM EDTA, 1 mg/mL proteinase K). After agarose gel electrophoresis, the digested DNA products were detected by a Typhoon phosphor imaging system. Purified HTT/mHTT proteins are purchased from Coriell Institute. Recombinant Exo1 and MutLα proteins were expressed in insect cells and purified, as described (80). For in vivo end resection assays, ER-AsiSI U2OS cells expressing Flag–HTT–exon1–23Q and Flag–mHTT–exon1–73Q were treated with 900 nM 4-OHT for 4 h to induce a DSB at the AaiSI site. Genomic DNA (10 ng) was used to determine the percentage of ssDNA generated during DNA end resection at various BsrGI sites (Fig. 4*F*) by the Taqman qPCR reactions using primers and probes specific for DSB1-335, DSB1-1618, and DSB1-3500 (*SI Appendix*, Table S1). The percentage of resection-generated ssDNA was calculated using the formula ssDNA% = 1/[2^(ΔCt - 1) + 0.5]*100.

HD Animals and Tissue Collection. Male Q175 HD knock-in mice were obtained from JAX (Strain #:027410) and bred with C57BL/6 WT females (JAX 000664) to set up the colony. All mice were maintained and bred under standard conditions consistent with NIH guidelines and approved by the University of California, Los Angeles Institutional Animal Care and Use Committees. The cages were maintained on a 12:12 light/dark cycle, with food and water ad lib. Four wild-type and four heterozygous Q175 (two males and two females each) were killed at 10 mo of age. Brains were removed, sliced, and micro-dissected on ice. Striatal tissues were collected and fresh frozen on dry ice.

Quantification and Statistical Analysis. Two-tailed Student's paired or unpaired *t* test was used for two-group comparisons, and one-way ANOVA was used for comparing more than two groups. A *P*-value of less than 0.05 was considered statistically significant. Data were represented as means ± SEM. All graphs and analyses were performed using GraphPad Prism statistical software (GraphPad Software).

Data, Materials, and Software Availability. All study data are included in the article and/or *SI Appendix*.

ACKNOWLEDGMENTS. This work was partially supported by grants from the Hereditary Disease Foundation (HDF) (GAA202008) and the Cancer Prevention & Research Institute of Texas (CPRIT, RR160101). G.-M.L. is a CPRIT Scholar in Cancer Research and the holder of the Reece A. Overcash, Jr. Distinguished Chair for Research on Colon Cancer. X.W.Y. is supported by NINDS (R01NS113612), CHDI, and HDF.

Author affiliations: [a]Department of Radiation Oncology, University of Texas Southwestern Medical Center, Dallas, TX 75390; [b]The Ministry of Education Key Laboratory of Reproductive Genetics, Department of Reproductive Endocrinology, Women's Hospital, Zhejiang University School of Medicine, Hangzhou 310006, China; [c]Cui-ying Experimental Center, Lanzhou University Second Hospital, Lanzhou 730030, China; [d]Center for Neurobehavioral Genetics, Semel Institute for Neuroscience & Human behavior, University of California, Los Angeles, CA 90095; [e]Department of Psychiatry and Biobehavioral Sciences, David Geffen School of Medicine, University of California, Los Angeles, CA 90095; [f]Institute for Cancer Research, Chinese Institutes for Medical Research, Beijing 100069, China; and [g]School of Basic Medical Sciences, Capital Medical University, Beijing 100069, China

1. E. Scherzinger *et al.*, Huntingtin-encoded polyglutamine expansions form amyloid-like protein aggregates in vitro and in vivo. *Cell* **90**, 549–558 (1997).
2. K. Sathasivam *et al.*, Aberrant splicing of HTT generates the pathogenic exon 1 protein in Huntington disease. *Proc. Natl. Acad. Sci. U.S.A.* **110**, 2366–2370 (2013).
3. E. Cattaneo, C. Zuccato, M. Tartari, Normal huntingtin function: an alternative approach to Huntington's disease. *Nat Rev. Neurosci.* **6**, 919–930 (2005).
4. D. Rigamonti *et al.*, Wild-type huntingtin protects from apoptosis upstream of caspase-3. *J. Neurosci.* **20**, 3705–3713 (2000).
5. F. Saudou, S. Finkbeiner, D. Devys, M. E. Greenberg, Huntingtin acts in the nucleus to induce apoptosis but death does not correlate with the formation of intranuclear inclusions. *Cell* **95**, 55–66 (1998).
6. H. Zhang *et al.*, Full length mutant huntingtin is required for altered Ca2+ signaling and apoptosis of striatal neurons in the YAC mouse model of Huntington's disease. *Neurobiol. Dis.* **31**, 80–88 (2008).
7. D. Yang *et al.*, Expression of Huntington's disease protein results in apoptotic neurons in the brains of cloned transgenic pigs. *Hum. Mol. Genet.* **19**, 3983–3994 (2010).
8. M. Chen *et al.*, Minocycline inhibits caspase-1 and caspase-3 expression and delays mortality in a transgenic mouse model of Huntington disease. *Nat. Med.* **6**, 797–801 (2000).
9. V. Maglione, M. Cannella, R. Gradini, G. Cislaghi, F. Squitieri, Huntingtin fragmentation and increased caspase 3, 8 and 9 activities in lymphoblasts with heterozygous and homozygous Huntington's disease mutation. *Mech. Ageing Dev.* **127**, 213–216 (2006).
10. M. Bjorkqvist *et al.*, A novel pathogenic pathway of immune activation detectable before clinical onset in Huntington's disease. *J. Exp. Med.* **205**, 1869–1877 (2008).
11. A. Dalrymple *et al.*, Proteomic profiling of plasma in Huntington's disease reveals neuroinflammatory activation and biomarker candidates. *J. Proteome Res.* **6**, 2833–2840 (2007).
12. E. Wild *et al.*, Abnormal peripheral chemokine profile in Huntington's disease. *PLoS Curr.* **3**, RRN1231 (2011).
13. M. Sharma, S. Rajendrarao, N. Shahani, U. N. Ramirez-Jarquin, S. Subramaniam, Cyclic GMP-AMP synthase promotes the inflammatory and autophagy responses in Huntington disease. *Proc. Natl. Acad. Sci. U.S.A.* **117**, 15989–15999 (2020).
14. A. Jauhari *et al.*, Melatonin inhibits cytosolic mitochondrial DNA-induced neuroinflammatory signaling in accelerated aging and neurodegeneration. *J. Clin. Invest.* **131**, 3124–3136 (2021).

15. A. Ablasser, Z. J. Chen, cGAS in action: Expanding roles in immunity and inflammation. *Science* **363**, eaat8657 (2019).
16. K. J. Mackenzie *et al.*, cGAS surveillance of micronuclei links genome instability to innate immunity. *Nature* **548**, 461–465 (2017).
17. T. Li, Z. J. Chen, The cGAS–cGAMP–STING pathway connects DNA damage to inflammation, senescence, and cancer. *J. Exp. Med.* **215**, 1287–1299 (2018).
18. Y. Bordon, Innate immunity: Nuclear waste ignites cGAS. *Nat. Rev. Immunol.* **17**, 533 (2017).
19. A. C. Chin, Neuroinflammation and the cGAS–STING pathway. *J. Neurophysiol.* **121**, 1087–1091 (2019).
20. T. Maiuri *et al.*, Huntingtin is a scaffolding protein in the ATM oxidative DNA damage response complex. *Hum. Mol. Genet.* **26**, 395–406 (2017).
21. R. Gao *et al.*, Mutant huntingtin impairs PNKP and ATXN3, disrupting DNA repair and transcription. *Elife* **8**, e42988 (2019).
22. Y. Enokido *et al.*, Mutant huntingtin impairs Ku70-mediated DNA repair. *J. Cell Biol.* **189**, 425–443 (2010).
23. X. H. Lu *et al.*, Targeting ATM ameliorates mutant Huntingtin toxicity in cell and animal models of Huntington's disease. *Sci. Transl. Med.* **6**, 268ra178 (2014).
24. J. Illuzzi, S. Yerkes, H. Parekh-Olmedo, E. B. Kmiec, DNA breakage and induction of DNA damage response proteins precede the appearance of visible mutant huntingtin aggregates. *J. Neurosci. Res.* **87**, 733–747 (2009).
25. J. L. Illuzzi, C. A. Vickers, E. B. Kmiec, Modifications of p53 and the DNA damage response in cells expressing mutant form of the protein huntingtin. *J. Mol. Neurosci.* **45**, 256–268 (2011).
26. H. Niu, S. Raynard, P. Sung, Multiplicity of DNA end resection machineries in chromosome break repair. *Genes. Dev.* **23**, 1481–1486 (2009).
27. F. Zhao, W. Kim, J. A. Kloeber, Z. Lou, DNA end resection and its role in DNA replication and DSB repair choice in mammalian cells. *Exp. Mol. Med* **52**, 1705–1714 (2020).
28. L. Ranjha, S. M. Howard, P. Cejka, Main steps in DNA double-strand break repair: An introduction to homologous recombination and related processes. *Chromosoma* **127**, 187–214 (2018).
29. G. M. Li, P. Modrich, Restoration of mismatch repair to nuclear extracts of H6 colorectal tumor cells by a heterodimer of human MutL homologs. *Proc. Natl. Acad. Sci. U.S.A.* **92**, 1950–1954 (1995).
30. J. Guan *et al.*, MLH1 deficiency-triggered DNA hyperexcision by exonuclease 1 activates the cGAS–STING pathway. *Cancer Cell* **39**, 109–121.e5 (2021).
31. Genetic Modifiers of Huntington's Disease (GeM-HD) Consortium, CAG Repeat not polyglutamine length determines timing of Huntington's disease onset. *Cell* **178**, 887–900.e14 (2019).
32. J. M. Lee *et al.*, A modifier of Huntington's disease onset at the MLH1 locus. *Hum. Mol. Genet.* **26**, 3859–3867 (2017).
33. R. M. Pinto *et al.*, Mismatch repair genes Mlh1 and Mlh3 modify CAG instability in Huntington's disease mice: Genome-wide and candidate approaches. *PLoS Genet.* **9**, e1003930 (2013).
34. K. Manley, T. L. Shirley, L. Flaherty, A. Messer, Msh2 deficiency prevents in vivo somatic instability of the CAG repeat in Huntington disease transgenic mice. *Nat. Genet.* **23**, 471–473 (1999).
35. S. Tome *et al.*, MSH3 polymorphisms and protein levels affect CAG repeat instability in Huntington's disease mice. *PLoS Genet.* **9**, e1003280 (2013).
36. A. Kantartzis *et al.*, Msh2–Msh3 interferes with Okazaki fragment processing to promote trinucleotide repeat expansions. *Cell Rep.* **2**, 216–222 (2012).
37. A. M. Gannon, A. Frizzell, E. Healy, R. S. Lahue, MutSbeta and histone deacetylase complexes promote expansions of trinucleotide repeats in human cells. *Nucleic Acids Res.* **40**, 10324–10333 (2012).
38. J. Guo, L. Gu, M. Leffak, G. M. Li, MutSbeta promotes trinucleotide repeat expansion by recruiting DNA polymerase beta to nascent (CAG)n or (CTG)n hairpins for error-prone DNA synthesis. *Cell Res.* **26**, 775–786 (2016).
39. N. Keogh, K. Y. Chan, G. M. Li, R. S. Lahue, MutSbeta abundance and Msh3 ATP hydrolysis activity are important drivers of CTG*CAG repeat expansions. *Nucleic Acids Res.* **45**, 10068–10078 (2017).
40. E. Dragileva *et al.*, Intergenerational and striatal CAG repeat instability in Huntington's disease knock-in mice involve different DNA repair genes. *Neurobiol. Dis.* **33**, 37–47 (2009).
41. F. Trettel *et al.*, Dominant phenotypes produced by the HD mutation in STHdh(Q111) striatal cells. *Hum. Mol. Genet.* **9**, 2799–2809 (2000).
42. Q. Ruan, M. Lesort, M. E. MacDonald, G. V. Johnson, Striatal cells from mutant huntingtin knock-in mice are selectively vulnerable to mitochondrial complex II inhibitor-induced cell death through a non-apoptotic pathway. *Hum. Mol. Genet.* **13**, 669–681 (2004).
43. M. J. Stoddart, Cell viability assays: Introduction. *Methods Mol. Biol.* **740**, 1–6 (2011).
44. I. Vermes, C. Haanen, H. Steffens-Nakken, C. Reutelingsperger, A novel assay for apoptosis. Flow cytometric detection of phosphatidylserine expression on early apoptotic cells using fluorescein labelled Annexin V. *J. Immunol. Methods* **184**, 39–51 (1995).
45. G. Galli, M. Fratelli, Activation of apoptosis by serum deprivation in a teratocarcinoma cell line: Inhibition by L-acetylcarnitine. *Exp. Cell Res.* **204**, 54–60 (1993).
46. P. J. Kong *et al.*, Increased expression of Bim contributes to the potentiation of serum deprivation-induced apoptotic cell death in Huntington's disease knock-in striatal cell line. *Neurol. Res.* **31**, 77–83 (2009).
47. P. Li *et al.*, Cytochrome c and dATP-dependent formation of Apaf-1/caspase-9 complex initiates an apoptotic protease cascade. *Cell* **91**, 479–489 (1997).
48. M. M. Xu *et al.*, Dendritic cells but not macrophages sense tumor mitochondrial DNA for cross-priming through signal regulatory protein alpha signaling. *Immunity* **47**, 363–373.e5 (2017).
49. E. Combes *et al.*, Inhibition of ataxia-telangiectasia mutated and RAD3-related (ATR) overcomes oxaliplatin resistance and promotes antitumor immunity in colorectal cancer. *Cancer Res.* **79**, 2933–2946 (2019).
50. L. Wu *et al.*, KDM5 histone demethylases repress immune response via suppression of STING. *PLoS Biol.* **16**, e2006134 (2018).
51. D. Korzhevskii, M. Karpenko, O. Kirik, Microtubule-associated proteins as indicators of differentiation and the functional state of nerve cells. *Neurosci. Behav. Physiol.* **42**, 215–222 (2012).
52. K. A. Sap *et al.*, Identification of full-length wild-type and mutant huntingtin interacting proteins by crosslinking immunoprecipitation in mice brain cortex. *J. Huntingtons Dis.* **10**, 335–347 (2021).
53. E. Cannavo, P. Cejka, S. C. Kowalczykowski, Relationship of DNA degradation by Saccharomyces cerevisiae exonuclease 1 and its stimulation by RPA and Mre11-Rad50-Xrs2 to DNA end resection. *Proc. Natl. Acad. Sci. U.S.A.* **110**, E1661–1668 (2013).
54. Y. Zhou, P. Caron, G. Legube, T. T. Paull, Quantitation of DNA double-strand break resection intermediates in human cells. *Nucleic Acids Res.* **42**, e19 (2014).
55. J. E. Nuss *et al.*, DNA damage induced hyperphosphorylation of replication protein A. 1. Identification of novel sites of phosphorylation in response to DNA damage. *Biochemistry* **44**, 8428–8437 (2005).
56. A. Marechal, L. Zou, RPA-coated single-stranded DNA as a platform for post-translational modifications in the DNA damage response. *Cell Res.* **25**, 9–23 (2015).
57. K. P. Bhat, D. Cortez, RPA and RAD51: Fork reversal, fork protection, and genome stability. *Nat. Struct. Mol. Biol.* **25**, 446–453 (2018).
58. P. T. Tran, N. Erdeniz, L. S. Symington, R. M. Liskay, EXO1-A multi-tasking eukaryotic nuclease. *DNA Repair (Amst)* **3**, 1549–1559 (2004).
59. L. B. Menalled *et al.*, Comprehensive behavioral and molecular characterization of a new knock-in mouse model of Huntington's disease: zQ175. *PLoS One* **7**, e49838 (2012).
60. E. E. Wanker, A. Ast, F. Schindler, P. Trepte, S. Schnoegl, The pathobiology of perturbed mutant huntingtin protein-protein interactions in Huntington's disease. *J. Neurochem.* **151**, 507–519 (2019).
61. M. Rieux *et al.*, Shedding a new light on Huntington's disease: how blood can both propagate and ameliorate disease pathology. *Mol. Psychiatry* **26**, 5441–5463 (2021).
62. F. Saudou, S. Humbert, The biology of Huntingtin. *Neuron* **89**, 910–926 (2016).
63. S. H. Stuwe *et al.*, Hepatic mitochondrial dysfunction in manifest and premanifest Huntington disease. *Neurology* **80**, 743–746 (2013).
64. J. C. L. Roy *et al.*, Somatic CAG expansion in Huntington's disease is dependent on the MLH3 endonuclease domain, which can be excluded via splice redirection. *Nucleic Acids Res.* **49**, 3907–3918 (2021).
65. J. Jiricny, The multifaceted mismatch-repair system. *Nat. Rev. Mol. Cell Biol.* **7**, 335–346 (2006).
66. F. A. Kadyrov, L. Dzantiev, N. Constantin, P. Modrich, Endonucleolytic function of MutLalpha in human mismatch repair. *Cell* **126**, 297–308 (2006).
67. K. E. Orii, Y. Lee, N. Kondo, P. J. McKinnon, Selective utilization of nonhomologous end-joining and homologous recombination DNA repair pathways during nervous system development. *Proc. Natl. Acad. Sci. U.S.A.* **103**, 10017–10022 (2006).
68. D. Merlo *et al.*, DNA repair in post-mitotic neurons: A gene-trapping strategy. *Cell Death Differ.* **12**, 307–309 (2005).
69. Y. Hong, T. Zhao, X. J. Li, S. Li, Mutant Huntingtin inhibits alphaB-crystallin expression and impairs exosome secretion from astrocytes. *J. Neurosci.* **37**, 9550–9563 (2017).
70. A. Decout, J. D. Katz, S. Venkatraman, A. Ablasser, The cGAS-STING pathway as a therapeutic target in inflammatory diseases. *Nat. Rev. Immunol.* **21**, 548–569 (2021).
71. X. Li *et al.*, Polymerases and DNA repair in neurons: Implications in neuronal survival and neurodegenerative diseases. *Front. Cell Neurosci.* **16**, 852002 (2022).
72. G. M. Li, The role of mismatch repair in DNA damage-induced apoptosis. *Oncol. Res.* **11**, 393–400 (1999).
73. H. Wang, C. W. Lawrence, G. M. Li, J. B. Hays, Specific binding of human MSH2.MSH6 mismatch-repair protein heterodimers to DNA incorporating thymine- or uracil-containing UV light photoproducts opposite mismatched bases. *J. Biol. Chem.* **274**, 16894–16900 (1999).
74. G.-M. Li, H. Wang, L. J. Romano, Human MutSa specifically binds to DNA containing aminofluorene and acetylaminofluorene adducts. *J. Biol. Chem.* **271**, 24084–24088 (1996).
75. J. Wu, L. Gu, H. Wang, N. E. Geacintov, G.-M. Li, Mismatch repair processing of carcinogen-DNA adducts triggers apoptosis. *Mol. Cell. Biol.* **19**, 8292–8301 (1999).
76. S. J. York, P. Modrich, Mismatch repair-dependent iterative excision at irreparable O6-methylguanine lesions in human nuclear extracts. *J. Biol. Chem.* **281**, 22674–22683 (2006).
77. J. Huang *et al.*, RAD18 transmits DNA damage signalling to elicit homologous recombination repair. *Nat. Cell Biol.* **11**, 592–603 (2009).
78. J. Ortega, G. S. Lee, L. Gu, W. Yang, G. M. Li, Mispair-bound human MutS–MutL complex triggers DNA incisions and activates mismatch repair. *Cell Res.* **31**, 542–553 (2021).
79. C. Han *et al.*, Tumor cells suppress radiation-induced immunity by hijacking caspase 9 signaling. *Nat. Immunol.* **21**, 546–554 (2020).
80. Y. Zhang *et al.*, Reconstitution of 5′-directed human mismatch repair in a purified system. *Cell* **122**, 693–705 (2005).